Two-body photodisintegration of ^{3}He between 150 and 350 MeV

D. I. Sober and Hall Crannell*
Department of Physics, The Catholic University of America, Washington, D.C. 20064

B. M. K. Nefkens
Department of Physics, University of California, Los Angeles, California 90024

W. J. Briscoe
Department of Physics, University of California, Los Angeles, California 90024 and Department of Physics, George Washington University, Washington, D.C. 20052†

D. H. Fitzgerald
Department of Physics, University of California, Los Angeles, California 90024 and Los Alamos National Laboratory, Los Alamos, New Mexico 87545†

R. Goloskie
Department of Physics, Worcester Polytechnic Institute, Worcester, Massachusetts 01609

W. W. Sapp, Jr.
William H. Bates Linear Accelerator, Department of Physics and Laboratory for Nuclear Science, Massachusetts Institute of Technology, Cambridge, Massachusetts 02139

(Received 10 August 1983)

Differential cross sections for ^{3}He(γ,d)^{1}H for incident energies between 150 and 350 MeV at center-of-mass proton angles near 60° and 90° have been measured with an absolute uncertainty of less than 6%. The experiment used a single-arm spectrometer, a gas target, and an uncollimated bremsstrahlung beam. The results are in good agreement with new measurements of the time-reversed reaction, ^{2}H(p,^{3}He)γ, giving no evidence for a violation of time-reversal invariance. The differential cross sections decrease smoothly with energy and show only a small contribution from the $\Delta(1232)$ resonance.

[NUCLEAR REACTIONS ^{3}He(γ,d)^{1}H, E_0=150–350 MeV; measured $d\sigma/d\Omega$ at θ_p(c.m.)≅60°, 90°; tested detailed balance and time-reversal invariance.]

I. INTRODUCTION

The two-body photodisintegration of ^{3}He

$$\gamma + {}^3\mathrm{He} \rightarrow \mathrm{p} + \mathrm{d} \ , \tag{1}$$

and its inverse reaction

$$\mathrm{p} + \mathrm{d} \rightarrow {}^3\mathrm{He} + \gamma \ , \tag{2}$$

at energies near the $\Delta(1232)$ resonance provide an excellent system for testing time-reversal invariance (TRI) and for studying the dynamics of the three-body system. Cross sections for reactions (1) and (2) were measured around 1970 at Caltech and Berkeley by Heusch *et al.*,[1,2] and the agreement of the cross sections with the detailed balance relationship was cited as evidence for TRI. However, other measurements of the cross section for reaction (1) (Refs. 3–6) disagree with the Caltech results by as much as a factor of 2 in either direction, and recent measurements of reaction (2) (Refs. 7 and 8) disagree, though less dramatically, with the earlier measurement. Such large discrepancies in the experimental data base have precluded meaningful tests of TRI and few-body calculations.

Time-reversal invariance implies that a reaction and its inverse (both averaged over polarizations) are related by detailed balance. For electromagnetic interactions of hadrons, however, current conservation prohibits the violation of detailed balance at the γ-N-N vertex, in which a real or virtual photon couples to a nucleon which remains on its mass shell.[9] Thus, at low energy, observation of detailed balance in electromagnetic interactions is a test of current conservation and not of TRI. At vertices such as γ-N-Δ and γ-N-N*, however, TRI is needed to ensure that detailed balance be satisfied. Meaningful tests of TRI by detailed balance in the electromagnetic interactions are therefore best performed in the resonance region, where these vertices play a significant role. Such tests have been performed using the reaction pairs $\gamma + \mathrm{d} \leftrightarrow \mathrm{n} + \mathrm{p}$,[10–14] $\gamma + \mathrm{n} \leftrightarrow \pi^- + \mathrm{p}$,[15–21] and, as mentioned above, $\gamma + {}^3\mathrm{He} \leftrightarrow \mathrm{p} + \mathrm{d}$.[1–8]

The detailed balance relationship between differential cross sections involving unpolarized particles at the same center-of-mass energy and angle is

$$\frac{d\sigma(a+b\rightarrow c+d)}{d\sigma(c+d\rightarrow a+b)} = \frac{(2S_c+1)(2S_d+1)p_c^{*2}}{(2S_a+1)(2S_b+1)p_a^{*2}} \ . \tag{3}$$

The factors $(2S+1)$ are the spin multiplicities, and p_a^* and p_c^* are the center-of-mass momenta in the initial and final two-body systems, respectively. (For the photon, $2S+1$ is replaced by two.) For the reactions listed above, the interpretation of the detailed balance tests has been made especially difficult by the lack of agreement among measurements of the *same* process. Of the three reaction

pairs, $\gamma + {}^3\text{He} \leftrightarrow \text{p} + \text{d}$ appears to be experimentally the most tractable as it involves neither a neutron beam nor the extraction of free-neutron cross sections from a deuterium target.

To resolve the large discrepancies among the four published data sets for ^{3}He photodisintegration at intermediate energies, we have performed a new measurement of this reaction using the MIT-Bates Linear Accelerator. The experimental approach was substantially different from those of the earlier measurements, and was chosen to minimize systematic errors. Preliminary results of this experiment have already been published.[22] The final results and a more detailed account of the experiment are presented here.

The present experiment differs from the previous measurements of ^{3}He(γ,p)d in several significant ways.

(i) Only the deuteron was detected. The deuteron production angle and momentum were measured in a high-resolution magnetic spectrometer. The single-arm technique eliminates the potential difficulties of acceptance matching inherent in a coincidence experiment, although special care is required to minimize and investigate backgrounds.

(ii) A gas target was used, eliminating the uncertainties involved in controlling and measuring the density of a liquid ^{3}He target. The target thickness was a small fraction of that of the liquid targets used in each of the previous experiments, greatly reducing the effects of energy loss and multiple scattering of the outgoing deuteron.

(iii) The incident photon beam was the full, uncollimated bremsstrahlung beam produced by a well-calibrated electron beam in a thin radiator of known composition and thickness. This allowed the absolute flux to be determined independently of quantameter calibrations and eliminated the possibility of introducing a net polarization of the photons as a result of collimation. Production of secondary particles in the beam by photon interactions in collimators was avoided, and the beam-target interaction volume was well-defined and small. Because the electron beam passed through the target, measurement and subtraction of electron-induced events was necessary.

(iv) The momentum calibration of the spectrometer was checked repeatedly during the experiment. This allowed the incident photon energy of each event to be determined accurately, a matter of considerable importance in measuring a cross section which varies rapidly with energy.

(v) With minor changes the spectrometer could be used to select electrons, protons, deuterons, tritons, or ^{3}He's. This feature allowed us to test the normalization factors used in calculating the cross section, and to measure the purity and density of the target gas by elastic electron scattering.

(vi) Cross sections were measured at a number of electron beam energies with overlapping photon-energy ranges.

In Sec. II we discuss the experimental technique in more detail. The analysis of the data is described in Sec. III, and the results are presented in Sec. IV along with comparisons to theory and to other experiments.

II. EXPERIMENTAL METHOD

A. Photon beams

Cross sections were measured at two deuteron laboratory angles, 72.0° and 103.0°, corresponding to proton center-of-mass angles of approximately 90° and 60°, respectively. For each angle, measurements were made using electron beams of four energies: 275, 300, 325, and 360 MeV at 72°, and 210, 260, 310, and 360 MeV at 103°. Bremsstrahlung photons were produced in a thin radiator foil located inside the scattering chamber (Fig. 1), 15 cm from the center of the ^{3}He target. Tantalum was chosen as the radiator material after some early test runs were made using both tantalum and aluminum radiators. For the same thickness in radiation lengths, an Al radiator of greater areal density is required, producing a significantly higher empty-target background.

The cross section measurements were made using a tantalum radiator foil 235 mg/cm^2 (0.0354 radiation length) thick. For comparison, additional measurements were made with tantalum radiators of thicknesses 93 and 441 mg/cm^2 (0.0137 and 0.0656 radiation lengths) or with a 284 mg/cm^2 copper radiator (0.0221 radiation lengths). The thickness of each foil was determined by weighing. A sample of the standard Ta radiator foil was determined by mass-spectroscopic analysis to consist of more than 99.9% Ta. A thin (35 mg/cm^2 or 0.0009 radiation length) BeO screen attached to the downstream face of the standard 0.035-radiation-length tantalum radiator was viewed by a television camera in order to monitor the size and position of the electron beam on the radiator. The thickness of the BeO screen was included in the total radiator thickness used to calculate the photon spectrum.

Average beam currents in the range from 30 to 50 μA were used in the experiment. Two independent measurements were made of the flux of incident electrons on the radiator by integrating the current from two separate

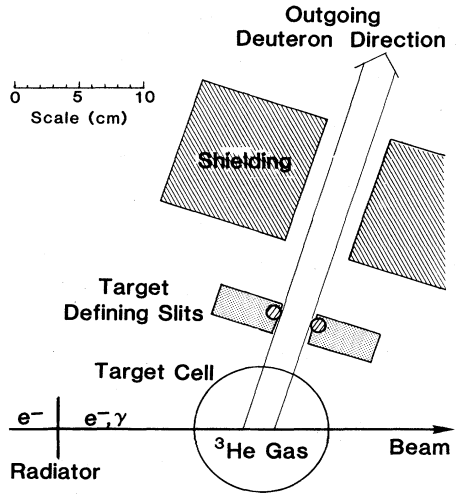

FIG. 1. Geometry of scattering chamber, including bremsstrahlung radiator, target cell, target defining slits, and shielding.

toroid beam monitors located between the beam switchyard and the target chamber. The toroids and integrators have been calibrated to the 0.1% level,[23] and under the conditions of this experiment are believed reliable to ±0.6%.

At each electron energy, measurements were made for a range of photon energies from at least 10 MeV above, to approximately 80 MeV below, the bremsstrahlung end point energy. Because of the short distance between the radiator and the gas target, all the photons produced in the radiator were incident on the target. Thus, only a calculation of the full angle-integrated bremsstrahlung spectrum was necessary, a much more accurate and reliable procedure than calculating the spectrum of a collimated photon beam, which depends on the angular acceptance.

The photon spectrum was calculated using computer codes based on three different parametrizations of thick-target bremsstrahlung.[24–26] The three spectra obtained agreed to within 0.7% over the entire photon spectrum to 10 MeV below the end point. (None of our reported results include data from the 10 MeV interval below the end point.) Because the thick-target corrections are small (<8%), the calculated spectra are as reliable as the thin-target Bethe-Heitler formula[25,27] with intermediate screening, to an accuracy of a few percent.

B. ^{3}He gas target

The ^{3}He gas was contained in a cylindrical aluminum cell of 10 cm diam with its axis vertical. The target cell was a copy of the target used by Dunn *et al.*[28] in a measurement of elastic electron scattering from ^{3}He. It was constructed by machining a 0.40-mm-thick, 38-mm-high window in a thick-walled aluminum cylinder which was welded to a solid aluminum plate on the bottom and to a liquid nitrogen reservoir above. Gas was transferred between the target cell and a storage cylinder through a thin transfer line by means of a diaphragm pump. The filling procedure consisted of evacuating the target and fill lines, filling with room temperature gas, recording the target pressure, cooling with liquid nitrogen, and recording the final pressure. In both cases, pressures were recorded after thermal equilibrium was reached.

During the experiment the target was emptied and filled several times; the gas pressure in the target was slightly different after each filling and was typically 1.03 MPa, measured to ±0.3%. The temperature of the target gas was calculated to be 80.6±1.8 K based on the equilibrium pressure measurements made during the filling sequence. The target density was calculated from the temperature and pressure of the gas; the typical density was about 4.6 mg/cm^3. The target cell was valved off from the storage tank, so that the quantity of gas in the target remained constant during runs, although the temperature and pressure increased slightly as a result of beam heating. A small correction (less than 5%) was made for the variation in local density due to beam heating. This correction was based on our measurements of electron scattering at various beam rates, and agrees with previous results obtained with this target system.[28]

The purity of the gas was reported by the supplier[29] as greater than 99.9%. The recoil-energy resolution of our electron scattering measurements was adequate to provide an on-line mass analysis of target composition for light nuclides. The target impurities observed in the spectra were a poorly resolved multiple peak in the carbon-nitrogen-oxygen region, corresponding to less than 0.05% by mass, and a ^{4}He component which increased from 0.6% to 1.0% by mass in the course of the experiment. A mass-spectroscopic analysis of a gas sample after the experiment corroborated the latter ^{4}He value. The increase in ^{4}He content is thought to be due to small amounts of ^{4}He not purged from the system prior to the various ^{3}He fillings, and to diffusion through the rubber diaphragm during pumping.

C. Spectrometer and detector system

Deuterons were detected in the Bates 900-MeV/c high-resolution spectrometer.[30] The trigger required a twofold or threefold coincidence in a set of five plastic scintillation counters,[31] of thicknesses 1.6, 3.2, 12.7, 12.7, and 12.7 mm (Fig. 2). The deuteron momentum was measured by a set of multiwire chambers in the focal plane region.[32] Because high resolution was not necessary for our measurements, only the coarse momentum channels (each corresponding to one of the 100 wires of the vertical drift chamber without software interpolation) were used. This results in a channel width of 0.06% in deuteron momentum. The photon energy was calculated from the deuteron kinematics: the bin width in photon energy was less than 0.5 MeV. The photon energy resolution was dominated by the angular acceptance of the spectrometer and

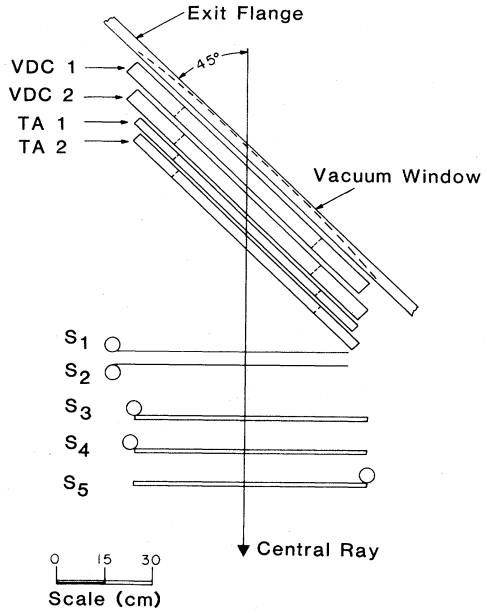

FIG. 2. Detectors in the focal-plane region of the Bates 900 MeV/c spectrometer. VDC and TA are the multiwire chambers which provide spatial information, and S_1–S_5 are plastic scintillation counters.

the finite target size, and varied from 1.2 to 4.5 MeV FWHM.

The usable momentum acceptance of the spectrometer was $\pm 2.8\%$. In order to cover the desired photon energy ranges, the spectrometer magnetic field was varied in overlapping steps. The magnetic field was measured by a nuclear magnetic resonance (NMR) probe in each of the two dipole magnets which compose the spectrometer. The calibration of the spectrometer field was verified by means of measurements of elastic electron scattering and by an evaluation of the bremsstrahlung end point energy in ^{3}He$(\gamma,\mathrm{d})^1$H spectra.

The angular acceptance of the spectrometer was determined by two pairs of remotely driven jaws which define the horizontal and vertical apertures. The spectrometer jaws were set to define a solid angle of 2.00 msr (± 7.9 mrad horizontal by ± 63.4 mrad vertical) at the center of the target cell. A steel-and-tungsten slit with a 2.54 cm horizontal aperture was used inside the scattering chamber to prevent the spectrometer from viewing the target cell windows (Fig. 1). These apertures defined a product of target length times solid angle which was equal to 5.61 cm msr when the spectrometer angle was 72° and 5.48 cm msr at 103°, each known to a precision of $\pm 2\%$. The edges of the target-defining slit consisted of cylindrical tungsten rods 0.95 cm in diameter. Each rod was embedded in, and protruded 0.76 mm from, a steel block 2.54 cm thick whose inner faces sloped outward toward the spectrometer to eliminate slit face scattering. The use of dense material to form the slit minimizes particle penetration of the slit edges; penetration by deuterons with momenta in the spectrometer acceptance range was calculated to contribute a background of no more than 0.7% under the conditions of the experiment.

For each event, spatial information from the focal plane chambers and pulse heights from the five scintillation counters were recorded. Discriminator thresholds were set well below the pulse height for deuterons at each spectrometer field setting. The event trigger accepted all deuterons, as well as many protons which were easily rejected in subsequent analysis.

D. Run procedures

The measurements at two spectrometer angles and four end point energies at each angle result in eight data sets which compose the main part of the experiment. Four or five overlapping magnetic field settings were used at each end point energy in order to measure the desired range of photon energies. For each data set and field setting, four different types of runs were required:

(1) radiator in, target full (IF);
(2) radiator out, target full (OF);
(3) radiator in, target empty (IE);
(4) radiator out, target empty (OE).

The IF runs include the true ^{3}He(γ,d)p events. The OF runs measure the yield due to electron interactions in the target, which are also present in the IF runs and must be subtracted by a procedure described in Sec. III. The IE and OE runs measure a small background which is subtracted from the full-target data.

In addition to the main data set described above, several auxiliary data sets were taken for the purpose of calibration and testing. These measurements include the following:

(i) runs in which only a single parameter was changed, such as radiator thickness and material, gas pressure, or spectrometer acceptance; (ii) elastic electron scattering from ^{3}He; (iii) deuteron photodisintegration: ^{2}H(γ,p)n; (iv) ^{4}He$(\gamma,^3\mathrm{H})^1$H; and (v) ^{4}He(γ,d).

The experimental changes required for these supplementary measurements were small, consisting only of changing the target gas, adjusting the gain on the scintillator output pulses, or, for the electron scattering measurements, reversing the spectrometer field.

III. ANALYSIS AND TESTS

A. Event reconstruction and selection

The measurement of the angle and energy of the deuteron is sufficient to determine the kinematics of a ^{3}He(γ,d)p event. (Deuterons produced in multiparticle final states, such as d-N-π, are kinematically excluded for photon energies within 120 MeV of the end point.) The crux of the experiment is the ability to ascertain that the detected particle is, in fact, a deuteron. The deuteron energy was always greater than 38 MeV, enough to pass through at least two of the five trigger counters. For particles of equal momentum, as selected by the spectrometer, the ionization energy loss of a deuteron was about twice that of a proton and $\frac{2}{3}$ that of a triton, so that the pulse height data in several counters provided the basis for a clean separation of deuterons from background particles.

Figure 3(a) shows the distribution of raw events according to pulse height and momentum in counter 1. Distinct groups corresponding to protons, deuterons, and tritons are clearly seen. As the discriminator threshold for each of the trigger counters was set safely below the deuteron distribution, many protons were accepted. The observed tritons cannot be produced by any one-step reaction on ^{3}He, and originate in the target walls. Even if they were not rejected on the basis of pulse height, most tritons would be eliminated by the empty-target subtraction. The slope and curvature of the particle distributions are due primarily to the attenuation of light in the long scintillation counters. The pulse height was corrected to a position-independent value by means of empirical correction functions fitted to the data. After correction, the deuteron events form a distinct peak in each counter. When pulse heights in two counters are correlated [Fig. 3(b)], the deuterons are even more easily identified. The final selection of deuteron events was made on the basis of cuts on corrected pulse height correlated in two or more counters. A small number of events, normally fewer than

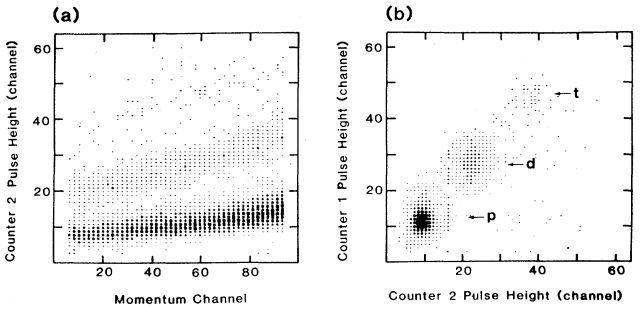

FIG. 3. (a) Distribution of events versus momentum and pulse height in scintillation counter 1. Higher channel number corresponds to lower momentum. (b) Distribution of events versus pulse heights in scintillation counters 1 and 2. The pulse heights have been corrected for light attenuation as a function of position in the focal plane.

1%, did not fall neatly into a particle classification, having deuteronlike pulse heights in the upstream counters but anomalously high pulse heights in the downstream counters. These were interpreted as due to deuterons interacting in the upstream counters and were accepted.

The selection cuts were determined separately for each radiator-in, full-target run (category IF defined in Sec. II D). For the background runs (OF, IE, and OE), which had far fewer events, cuts were made using the values determined for the associated IF run.

The events which passed these cuts were then normalized to the total charge of the incident electron beam as measured by the beam toroid integrators and corrected for losses due to dead time and detector inefficiencies. During a typical beam pulse of 15 μs width and 6 to 10 mA peak current, there were typically several background events in the wire chambers uncorrelated with a valid trigger signal. If one of these events occurred within $\sim$300 ns of a good event, it had a high probability of confusing the delay-line electronics and causing the event to be rejected in the subsequent analysis. Wire chamber inefficiencies result in a similar rejection. A simple algorithm, whose applicability was checked by examining the raw data from the drift chamber delay lines, was used to correct for these rejected events. Another type of dead time arises because the electronics could not digitize more than one set of scintillator signals per beam burst. By counting the number of such unanalyzed events (usually less than 3%) one can correct in a straightforward manner for these losses. The total correction for both categories was normally between 3% and 5%, ranging up to 12% in a few runs at the highest counting rate.

B. Event subtraction

The radiator-in, full-target runs (IF runs) contain two types of deuteron background: (i) deuterons produced in multistep reactions, or rescattered after production, and (ii) events induced by the electron beam passing through the ^{3}He target, either via additional real photons produced in the target walls and gas, or through the electrodisintegration reaction ^{3}He(e,e'd)p. The latter process is the dominant background; a simple calculation using the Dalitz-Yennie virtual photon model[33] predicts the (e,e'd) contribution to be approximately 30% of the total event rate with the standard tantalum radiator. When the radiator is removed (as in the OF runs), electrodisintegration is the dominant process.

In the limit of an infinitely thin radiator, the rate of good ^{3}He(γ,d)p events is given by the simple subtraction

$$R_{\rm in}-R_{\rm out}=(R_{\rm IF}-R_{\rm IE})-(R_{\rm OF}-R_{\rm OE})\ . \tag{4}$$

The last four subscripts refer to the categories defined in Sec. II D, and the rates are normalized as described in Sec. III A. The relative magnitudes of the four rates are shown in Fig. 4(a). The spectra have been converted from the form $R(P)$, where P is the deuteron momentum, into the form $R(k)$, where k is the *effective photon energy,* i.e., the energy of a photon required to produce a deuteron of the given momentum P at the specified angle via the reaction ^{3}He(γ,d)p. For both photodisintegration and electrodisintegration events, k must be less than the electron beam energy. The end point is clearly discernible in the full-target rates (IF and OF) of Fig. 4(a).

The finite thickness of the radiator complicates this subtraction, as the electrons which pass through the ^{3}He target in the IF and IE runs have been degraded in energy by the radiator, and thus produce a slightly different spectrum of deuterons than do the undegraded electrons in the OF and OE runs. The electron-induced counting rate in a spectrum bin is a function of both the effective photon energy k and the electron energy E. For a bin of effective photon energy k, the desired subtraction is

$$R_\gamma(k,E)=R_{\rm in}(k,E_0)-\int_k^{E_0} R_{\rm out}(k,E)(dN/dE)dE\ , \tag{5}$$

where E_0 is the incident electron energy and dN/dE is the differential energy spectrum of electrons emerging from

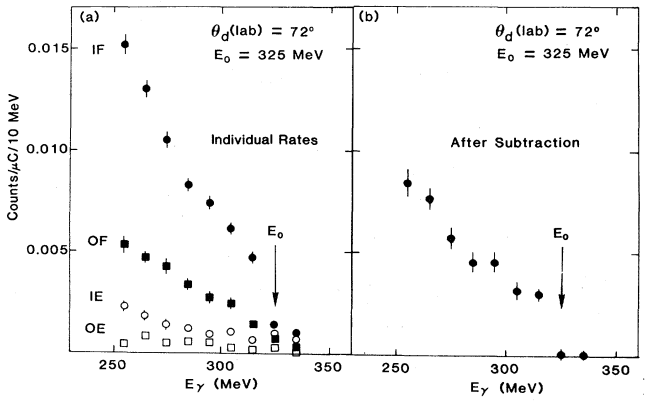

FIG. 4. (a) Spectra of the four raw data categories described in the text: IF (radiator in, target full), IE (radiator in, target empty), OF (radiator in, target full), and OE (radiator in, target empty). (b) Spectrum after the subtraction described by Eq. (5).

the radiator. The quantity dN/dE can be calculated by the simple formula[34]

$$dN/dE=[E_0\Gamma(t')]^{-1}[\ln(E_0/E)]^{t'-1}, \quad (6)$$

where Γ is the gamma function, and t' is the radiator thickness in radiation lengths divided by ln2. This formula is not significantly different from more elaborate formulas quoted by Tsai[25]; its adequacy was verified by means of a Monte Carlo shower calculation using the Stanford EGS code.[35] The integral in Eq. (5) was evaluated numerically using 5-MeV bins. The integrand for the highest-E bin (which includes more than 80% of the electrons) was evaluated using $R_{\text{out}}(k,E_0)$. For the lower-E bins, $R_{\text{out}}(k,E)$ was approximated by fitting empirical curves to the data taken at the four values of E_0; the variation with E over the necessary range is small enough that one can be confident of the extrapolation. The degraded-energy subtraction of Eq. (5) typically results in a 5% higher cross section than the simple subtraction given by Eq. (4). An example of the result of this subtraction is shown in Fig. 4(b).

As shown in Fig. 4, the region of effective photon energy above the end point has very few counts in the individual rates. Although most of this background is removed automatically by the subtractions discussed above, a small, apparently flat, residual background is observed above the end point in some runs. A constant background, equal to the average rate observed above the end point, was subtracted from the radiator-in and radiator-out data separately. This adjustment resulted in a reduction of 1–6% in the event rate for the highest energy bin of each subtracted spectrum, and had a much smaller effect on the lower energy bins. (The absence of more significant backgrounds is demonstrated in Sec. III F below.)

C. Energy calibration

As can be seen from the raw and subtracted spectra of Fig. 4, the counting rates for this reaction are strongly dependent on photon energy. For this reason, it is essential that the photon energy of each event be well known. In our experiment, the photon energy was determined by reconstruction of the two-body kinematics of the event using the deuteron momentum and angle. In order to test the photon energy reconstruction, we performed least-squares fits to the event spectrum in the end point region, with the end point energy as one of the varied parameters, using the theoretical bremsstrahlung spectrum shape near the end point,[26] corrected for resolution, and a simple parametrization of the cross section. Despite the limited statistics, the end point energy can be fit with a statistical uncertainty of less than ± 1 MeV (Fig. 5). In all cases the result is within 2 MeV of the beam energy as determined from the beam switchyard magnet calibrations. The beam energy was also confirmed by the electron scattering measurements which were made during our experiment. Combining the results of all runs, we obtain an uncertainty of ± 1.2 MeV in our reconstructed photon energy, far better than in previous measurements of this reaction.

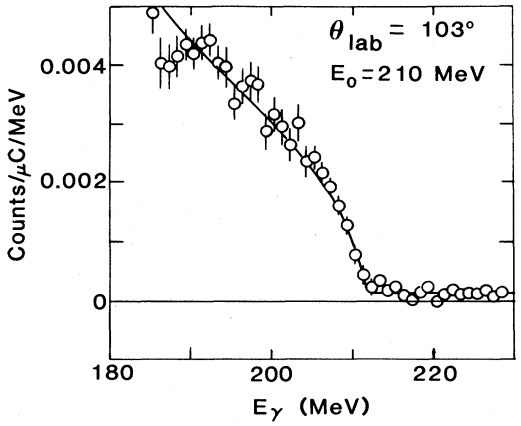

FIG. 5. Spectrum of events (radiator in) near the bremsstrahlung end point. The solid curve is the result of a least-squares fit which was used to determine the end point energy (212.1±0.2 MeV).

D. Cross section calculation

The differential cross section for the bin of photon energy $k\pm\Delta k/2$ is

$$d\sigma/d\Omega=\epsilon\frac{Y(k)J(k,\theta)}{N_\gamma(k)\rho(L\Delta\Omega)}, \quad (7)$$

where $Y(k)$ is the net number of good events in each bin (corrected for dead time and chamber inefficiency), ρ is the target gas density, $L\Delta\Omega$ is the product of target length viewed by the spectrometer and the spectrometer solid angle (Sec. II C), and

$$J(k,\theta)=d\Omega(\text{lab})/d\Omega(\text{c.m.})$$

is the kinematic conversion factor from laboratory to center-of-mass cross sections. $N_\gamma(k)$ is the number of incident photons in the energy interval Δk (10 MeV in our analysis). It is proportional to the integrated electron charge, the radiator thickness, and the bremsstrahlung spectrum calculated as described in Sec. II A. The factor ϵ contains the following small corrections to the cross section:

(i) deuteron losses through interactions in the target wall, spectrometer end window, chambers, and upper counter (1.5%);

(ii) reduction of the local gas density in the target because of beam heating (3.8–5.5%);

(iii) contributions of 1.5–3.7% from the ^{4}He and heavier impurities in the target gas based on the measured contaminations and on measurements of the yield of deuterons from a ^{4}He-filled target.

The normalization factors and uncertainties are summarized in Table I.

TABLE I. Normalization constants, corrections, and uncertainties.

	Units	$\theta_d=72°$	$\theta_d=103°$
Factor			
Target density	mg/cm^3	4.59±0.10 to 4.64±0.10	4.48±0.10 to 4.58±0.10
Target length × solid angle	cm msr	5.61±0.11	5.48±0.11
Correction			
Events from target impurities	%	−3.1±0.7 to −3.7±0.7	−1.5±0.3 to −1.8±0.3
Beam heating of target gas	%	+3.8±1.2 to +5.5±1.6	+4.4±1.3 to +5.5±1.6
Deuteron interaction	%	+1.5±0.5	+1.5±0.5
Dead time and chamber efficiency	%	+2.9±1.0 to +10.4±2.0	+2.8±1.0 to +7.9±2.0
Other uncertainties			
Electron flux		±0.6%	±0.6%
Tantalum radiator thickness		±0.5%	±0.5%
Bremsstrahlung spectrum		±2.0%	±2.0%
Particle identification		±1.0%	±1.0%
Detector efficiency		±1.0%	±1.0%
Slit penetration		±0.3%	±0.3%
Energy scale (±1.2 MeV)		±1.6%	±1.0%
Background subtraction		±3.0%	±3.0%
Total systematic uncertainty		±5.8%	±5.7%

TABLE II. Tests of normalization.

External tests[a]

	θ_{lab}	E_0	Relative to results of Ref.	Ratio
^{3}He(e,e)	72°	180 MeV	28	1.02±0.02
^{3}He(e,e)	103°	210 MeV	28	0.98±0.04
^{2}H(γ,p)n	72°	250—320 MeV	10	1.10±0.08
			11	0.94±0.06
			12	0.94±0.06
			40	0.99±0.05
^{4}He(γ,t)p	103°	240—300 MeV	5	1.00±0.13
			41	0.99±0.09

Internal tests

	Expected ratio	Measured ratio
Thicker Ta radiator	1.765	1.748±0.088
Thinner Ta radiator	0.400	0.412±0.034
$d\sigma/d\Omega$ with Cu radiator compared to Ta radiator	1.00	1.03 ±0.05
Halve vertical acceptance	0.501	0.479±0.035
Halve horizontal acceptance	0.500	0.497±0.035
Reduce gas pressure	0.542	0.550±0.035

[a] Ratio of the cross section measured in this work to other published results. (Includes systematic errors in published results.)

E. Tests of normalization

Because of the wide variations among the previously reported measurements of this reaction, we felt it was imperative to calibrate our measurement in as many ways as possible within the allotted running time. Our comparisons were of two different types: "internal" (measurement of the same ^{3}He(γ,d)p cross section with different experimental parameters) and "external" (measurement of other reactions with only small changes in our experimental configuration). These tests are discussed below and summarized in Table II.

1. External tests

a. Elastic electron scattering. Measurements of elastic electron scattering from ^{3}He were made for incident energies of 180 MeV at 72° and 210 MeV at 103°. The elastically scattered electrons formed a background-free peak in the focal plane. The summed counts in the peak, corrected for radiative energy loss, yielded values of the ^{3}He elastic form factor [Fig. 6(a)] which agreed within 2% with the results of previous experiments.[28,36,37] The normalization of these experiments is not substantially in doubt because of the strong theoretical requirement that the distortion-corrected form factor extrapolate to one at zero momentum transfer. Thus, our measurements constituted a powerful check on several important factors in the ^{3}He(γ,d)p cross section: electron beam intensity, target density, effective target length, and solid angle. Including the quoted uncertainties of the previous measurements of ^{3}He(e,e) and the effects of the uncertainty in incident energy (<0.5 MeV), the sensitivity of this normalization test is better than 4%.

The (e,e) measurement afforded several additional checks on systematic effects.

(i) Target impurities were accurately determined by measuring the elastic scattering peaks due to the contaminants and comparing them to known elastic scattering cross sections for ^{4}He (Ref. 36) and ^{14}N.[38,39]

(ii) The position of the elastic peak in the focal plane checked the momentum calibration of the spectrometer and the energy calibration of the electron beam.

(iii) By varying the spectrometer field to step the elastic peak along the focal plane, we confirmed the uniformity of the efficiency of the chambers and scintillators.

(iv) By varying the electron beam current by a factor of 3, we checked the effects of beam heating on the target gas density.

b. Deuteron photodisintegration. Differential cross sections for d(γ,p)n were measured for photon energies between 250 and 320 MeV at 72° (approximately 90° in the c.m.s.). In this region, the most recent published measurements[10–12,40] of this process agree to within ±8%. Our measurement is fully consistent with these [Fig. 6(b)]. In this case, the factors tested also include the radiator thickness and the calculated bremsstrahlung spectrum. Our excellent agreement with the most recent measurement at Bonn,[40] using tagged photons, is especially significant, as the tagged-photon measurement is free of uncertainty in the photon flux, one of the limiting errors in any bremsstrahlung measurement.

c. Two-body photodisintegration of ^{4}He. A measurement of ^{4}He(γ,t)p was made with photon energies near 250 and 290 MeV, detecting the triton in the spectrometer at 103°. The resulting cross sections [Fig. 6(c)] agree well with published results from Saclay[5] and Bonn.[41] This

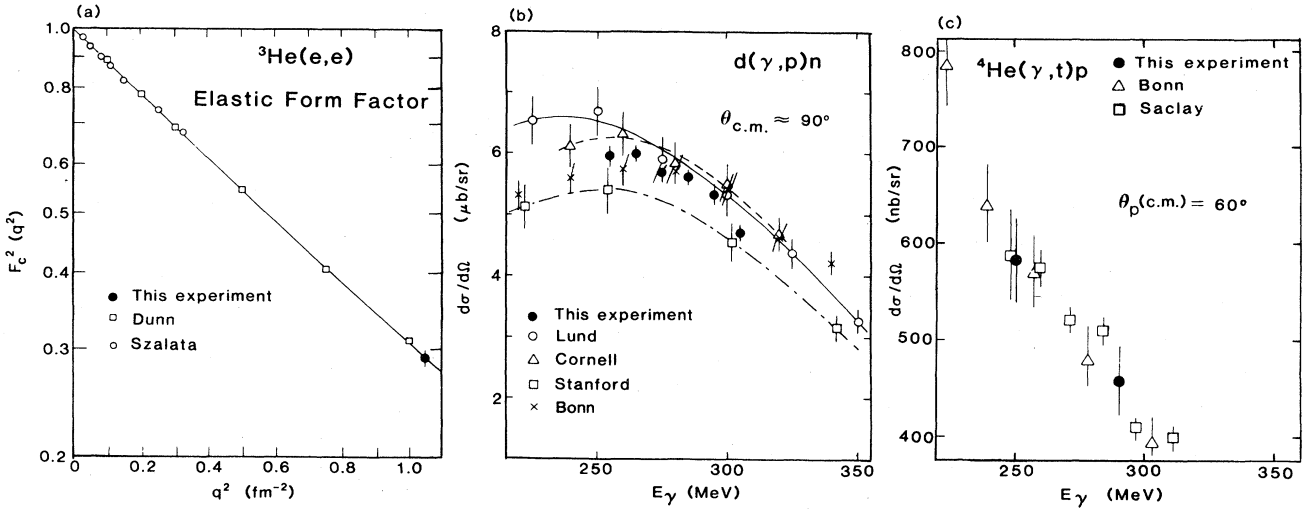

FIG. 6. Tests of normalization using measurements of other reactions taken during this experiment. (a) Form factor for elastic electron scattering from ^{3}He at 72° and 180 MeV, compared with charge form factor from Refs. 28 and 37. Our result has been reduced by 2.8% to correct for magnetic scattering, and its error bar includes the effects of energy uncertainty. (b) Cross section (with statistical errors) for deuteron photodisintegration at θ_p(lab)=72° [θ_p(c.m.)=86.4°–88.1°], compared with results (including systematic errors) of Refs. 10 (squares), 11 (triangles), 12 (open circles), and 40 (crosses), shifted to the same laboratory angle by means of their published angular distribution fits. The curves are drawn to guide the eye. (c) Cross section (with statistical errors) for ^{4}He(γ,t)p at θ_t(lab)=103° adjusted to θ_p(c.m.)=60°, compared with results (including systematic errors) of Refs. 5 (squares) and 41 (triangles).

provides an additional independent test of the overall normalization.

2. *Internal tests*

a. Variation of end point energy. For most measured photon energies, cross sections were obtained from data taken at two or more end point energies. If correctly measured, the photodisintegration cross section at a given photon energy must be independent of the end point energy of the bremsstrahlung beam, but in an experiment two types of end point dependent effects might be anticipated: those due to incorrect calculation of the bremsstrahlung spectrum, and those due to background events initiated by photons of higher or lower energy. In our data (Fig. 7), no significant end point dependence is seen: the data points measured at two or more end point energies are consistent, yielding a χ^2 of 9.7 for 11 degrees of freedom at 72° and 7.6 for 9 degrees of freedom at 103°. When compared with the statistical errors on the data points, this sets an upper limit of approximately 2% on background effects which have an end point dependence different from that of the good events.

b. Variation of radiator. The cross section data were taken with a 0.0354-radiation-length tantalum radiator foil, but some runs were repeated with thinner and thicker tantalum radiators, or with a copper radiator, as described in Sec. II. After subtraction, the number of events per incident electron was found to be exactly proportional to the photon flux calculated for each radiator, within the statistical uncertainties of 4—8% (Table II). This test is especially important as it sets severe upper limits on possible background processes, as discussed in detail below.

c. Variation of spectrometer aperture and target gas pressure. To search for other potential systematic effects, the horizontal and vertical spectrometer apertures and the target gas density were each reduced by a factor of approximately 2 for some test runs. The subtracted event rates in each case changed as expected (Table II), indicating no significant contributions from target vessel or slit rescattering.

F. Discussion of backgrounds

In a single-arm measurement of a low-cross-section reaction, it is necessary to take special care in investigating possible contamination of the good-event signal by background processes. In the present experiment, four classes of deuteron background events are possible, initiated by the following: (1) photons incident on ^{3}He, (2) photons incident on the target cell walls, (3) hadrons produced by real photons within the radiator foil, and (4) hadrons produced by virtual photons within the radiator. In each case, a subsequent interaction in the gas, target walls, or slits is necessary, as the spectrometer does not view the radiator or the target entry and exit windows directly. [Note that electron-induced events corresponding to classes (1) and (2) are eliminated by the radiator-out subtraction.] Background events of category (1) are due mainly to the slit scattering of deuterons (known to be small by our aperture-varying tests) and the production of deuterons by outgoing protons in the gas or target wall. The known cross sections for deuteron production by protons[42] precludes a contamination of more than 0.1% from this effect.

Process (2) can be stringently related to process (3) by

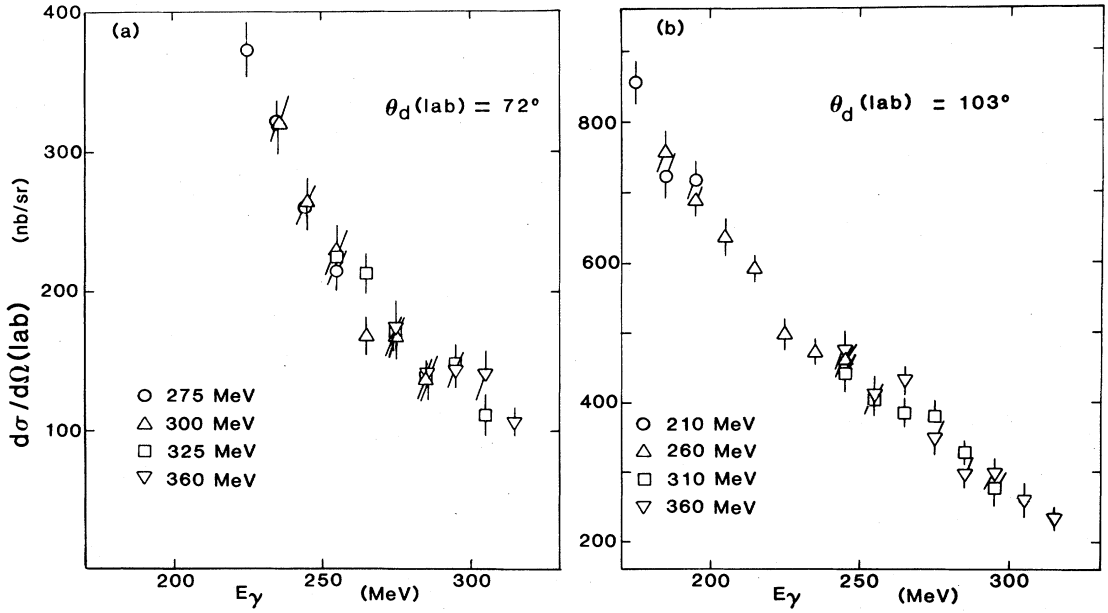

FIG. 7. Cross sections (in the laboratory system) measured using different bremsstrahlung end point energies. Error bars show statistical errors only.

the fact that the hadron production cross sections per nucleon are approximately the same in aluminum and tantalum, while the radiator is much thicker than the target wall. Thus, an upper limit on class (3) leads to a much smaller upper limit for class (2).

Because the virtual photon spectrum[33] is known to be roughly equivalent to bremsstrahlung from a real radiator of thickness 0.02 radiation lengths, the number of events of classes (3) and (4) must be roughly equal. Thus, an upper limit on *either* of these two background categories places firm limits on the *total* background present in the data. Backgrounds of type (3) have a unique experimental signal: they are proportional to the *square* of the radiator thickness t. Fitting a polynomial in t to the data taken at several radiator thicknesses (Fig. 8), we find an upper limit of 1.7% for the t^2 contribution at the normal radiator thickness. The small empty-target background shows a significant t^2 contribution which, however, has a negligible effect on the final results.

The absence of measurable background of this type is not surprising when specific examples are considered. We calculated the expected rate due to π^- photoproduction in the radiator followed by ^{3}He(π^-,d)n in the target gas, one of the few two-step processes that can produce deuterons of sufficiently high energy. Using cross section estimates based on experimental data,[43] we found a predicted contribution of no more than 0.1% of our good-event rate at any angle or energy.

From the agreement of the cross section measured at different end point energies, as well as the considerations discussed in this section, we are confident that the background contamination in our cross section is everywhere less than 3%, and contributes only modestly to the total systematic uncertainty.

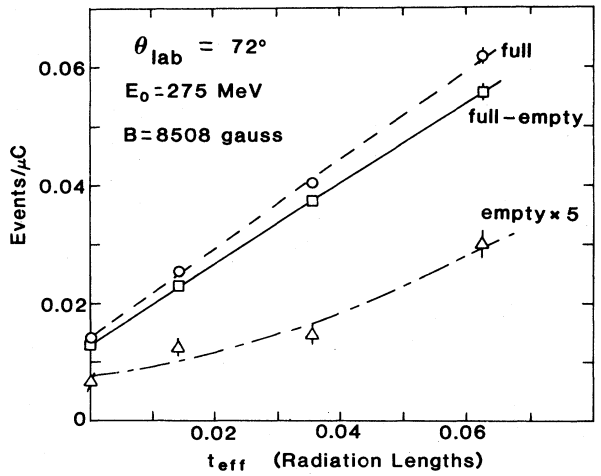

FIG. 8. Dependence of counting rates on radiator thickness. t_{eff} is the thickness in radiation lengths, corrected slightly so that the calculated number of photons per radiation length in the accepted photon energy interval is the same as for the 0.0354-radiation-length radiator.

IV. RESULTS

A. Comparison with other measurements and detailed balance

The cross sections obtained in this experiment, binned in 10-MeV intervals centered on the indicated photon energy, are plotted in Fig. 9 and tabulated in Table III. Measurements at different end point energies have been combined. The uncertainties quoted are statistical only; a systematic uncertainty of ±6% is not shown. The values plotted in Fig. 9 have been adjusted slightly so as to correspond to center-of-mass proton angles of exactly 60° and 90°. The angular adjustment factors are derived from the angular distributions of Refs. 4 and 6, and do not exceed 9%.

The results of previous measurements of ^{3}He(γ,p)d are also shown in Fig. 9. The present results are significantly higher than those of Saclay[5] and Bonn,[6] and lower than those of Caltech[1] and Frascati.[3] In Fig. 10 we compare our cross sections with the results of several measurements of the time-reversed reaction d(p,γ)^{3}He. The latter are multiplied by the detailed-balance factor of Eq. (3), $\frac{3}{2}(p^*/k^*)^2$, where p^* and k^* are the center-of-mass mo-

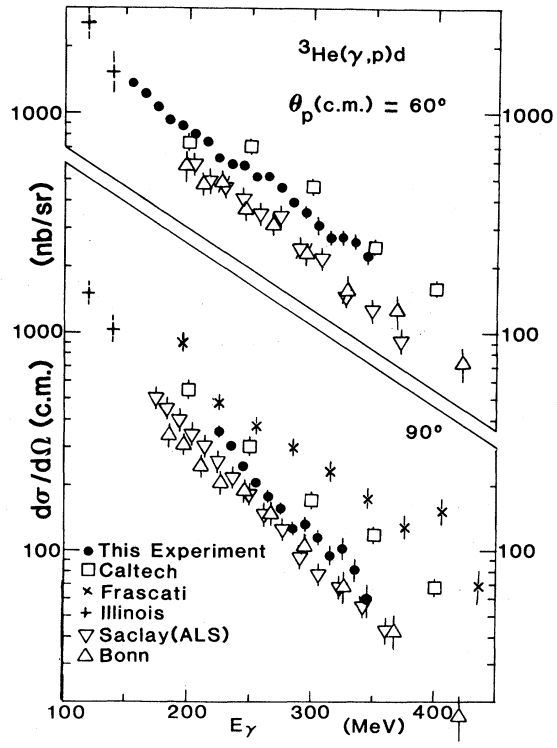

FIG. 9. Center-of-mass cross sections for $\gamma + {}^3\text{He} \rightarrow \text{p} + \text{d}$ measured in this experiment, adjusted to θ_p(c.m.)=60° and 90° (solid circles), compared with other measurements of this reaction: Refs. 1 (squares), 3 (×), 4 (+), 5 (inverted triangles), and 6 (triangles). The error bars for this experiment indicate statistical errors only, those for the other measurements indicate total error (statistical and systematic errors combined in quadrature).

TABLE III. Differential cross sections in the center-of-mass system for ^{3}He(γ,d)p at laboratory deuteron angles of 72° and 103°, determined for 10-MeV-wide bins of photon energy centered on the specified values of E_γ. The errors quoted are due to statistics only. There is an additional systematic uncertainty of ±6%.

	θ_d(lab)=103.05±0.02°		θ_d(lab)=72.01±0.02°	
E_γ (MeV)	θ_p(c.m.) (deg)	$d\sigma/d\Omega$ (nb/sr)	θ_p(c.m.) (deg)	$d\sigma/d\Omega$ (nb/sr)
155	64.0	1277±39		
165	63.6	1152±40		
175	63.2	1010±38		
185	62.9	885±25		
195	62.5	835±21		
205	62.2	767±32		
215	61.9	713±24		
225	61.6	599±28	92.9	325.4±16.9
235	61.3	570±23	92.6	280.4±10.9
245	61.0	563±18	92.3	229.0±10.5
255	60.7	507±22	92.0	193.7±8.5
265	60.4	510±18	91.7	167.8±9.1
275	60.1	459±21	91.4	149.4±8.4
285	59.8	396±17	91.1	121.1±7.8
295	59.6	360±20	90.9	127.8±8.6
305	59.3	318±31	90.6	112.1±9.0
315	59.0	283±21	90.3	93.7±9.2
325	58.8	285±23	90.1	101.6±11.4
335	58.5	278±22	89.8	81.8±9.6
345	58.3	242±22	89.6	60.5±10.6

menta of the proton and photon, respectively. While the agreement with the published data of Refs. 2 and 7 is poor, our data are in excellent agreement with recent data from TRIUMF.[8] We also note that new data from the UCLA-Saclay collaboration,[44] which differ from the published results of the earlier measurement by this same group,[7] are also in good agreement with our experiment.

With few exceptions, the measurements of ^{3}He(γ,p)d and d(p,γ)^{3}He agree at least qualitatively as to the shape of the energy and angular distributions in this region, differing primarily in normalization. The disagreement between our results and those of the previous ^{3}He(γ,p)d experiments is considerably greater than their estimates of systematic uncertainty (which are included in the plotted error bars). It is probable that some or all of these experiments have underestimated their systematic uncertainties. The most likely sources of error appear to be the determination of liquid target density and the calibration of the photon energy. Other factors common to previous experiments include the use of the following: (a) collimated photon beams, requiring more complicated and possibly less reliable calculations of the photon flux and quantameter calibrations, (b) thick targets in which the effects of multiple scattering and energy loss can be large, especially at low energies, and (c) range telescopes for detection of either the proton or deuteron, leading to substantial corrections for interactions in the range material. The present experiment is far less susceptible to such errors than its predecessors.

To illustrate the differences among the various measurements in this energy region, we have performed a

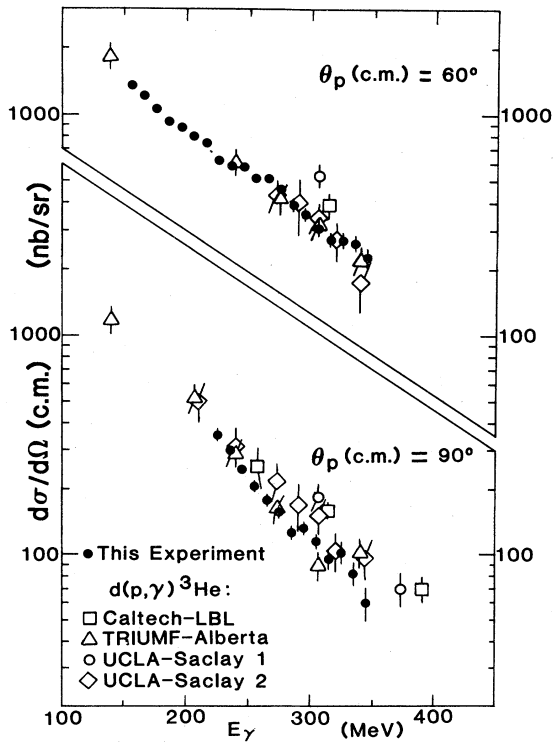

FIG. 10. Cross sections for $\gamma + {}^3\text{He} \rightarrow p + d$ measured in this experiment (solid circles) compared with measurements of the inverse reaction $p + d \rightarrow {}^3\text{He} + \gamma$ multiplied by the detailed balance factor: Refs. 2 (squares), 7 (open circles), 8 (triangles), and 44 (diamonds). The error bars for the other measurements include systematic errors.

quantitative comparison of the absolute value and energy dependence of each cross section. First, an empirical formula of the form

$$\frac{d\sigma}{d\Omega}=A\left[\frac{1}{E_\gamma}+\frac{B}{E_\gamma^2}+\frac{C}{(E_\gamma-D)^2+F^2}\right] \quad (8)$$

was fitted to the data points of this experiment at each of the two angles. The third term in brackets contributed negligibly, and the fit yielded a χ^2 of better than 1.2 per degree of freedom in each case. This function was then used as a reference shape, and was fitted to the data (with statistical uncertainties only) of the other ^{3}He(γ,p)d and d(p,γ)^{3}He experiments which fell in the energy range covered by our measurement, with only the overall factor A varied in the fit. The χ^2 of this fit thus describes the agreement of the relative energy dependence of the two experiments, while the ratio of the multiplicative factors

$$R=A(\text{other experiment})/A(\text{this experiment})$$

indicates the consistency of the absolute cross sections averaged over this energy region. For the radiative capture experiments, a ratio of 1 indicates agreement with the detailed balance relationship of Eq. (3). The results of these fits are shown in Table IV. The uncertainty in the ratio R includes the statistical uncertainty in the fits (multiplied by the square root of the χ^2 per degree of freedom when the latter exceeded 1) as well as the quoted systematic uncertainties of the experiments. When the present experiment is compared with the most recent d(p,γ)^{3}He results of TRIUMF (Ref. 8) and UCLA-Saclay,[44] no evidence is seen for a violation of detailed balance; the ratio is unity to an accuracy of better than 15%.

B. Comparison with theory

There are few theoretical calculations of ^{3}He(γ,p)d in the energy range of this experiment. Finjord[45] calculated the cross section between 165 and 330 MeV, using the Chew-Goldberger-Low-Nambu (CGLN) photoproduction amplitude[46] and a pseudoscalar πNN interaction to compute the two-nucleon pion-exchange contribution. The results are in approximate agreement with the Saclay data,[5] but are very sensitive to the choice of wave functions and to the assumptions about nucleon off-shell effects.

TABLE IV. Comparison of ^{3}He(γ,p)d and d(p,γ)^{3}He cross sections at θ_p(c.m.)=60° and 90°, using fits to the cross sections measured in this experiment.

Data set	χ^2 per DF[a]	No. of data points	Uncertainty in fit	Systematic uncertainty[b]	R[c]
		^{3}He(γ,p)d at 60° (E_γ=150–350 MeV)			
This expt	1.14	20	1.0%	6%	
Bonn (Ref. 6)	2.29	9	3.5%	10–15%	0.65±0.10
ALS (Ref. 5)	4.73	11	3.6%	10%	0.66±0.09
Caltech (Ref. 1)	21.1	5	7.7%	6%	1.16±0.42
		d(p,γ)^{3}He at 60°[d] (E_γ=150–350 MeV)			
TRIUMF (Ref. 8)	3.48	5	3.9%	12%	0.98±0.15
Saclay (Ref. 44)	2.30	8	4.5%	16%	0.97±0.18
Caltech (Ref. 2)		1	10%	1%	1.32±0.13
		^{3}He(γ,p)d at 90° (E_γ=220–350 MeV)			
This expt	0.85	13	2.4%	6%	
Bonn (Ref. 6)	6.09	5	5.9%	10–15%	0.72±0.15
ALS (Ref. 5)	2.60	10	1.1%	10%	0.75±0.09
Caltech (Ref. 1)	9.04	3	5.9%	6%	1.45±0.20
Frascati (Ref. 3)	19.2	5	11%	>5%	1.64±0.78
		d(p,γ)^{3}He at 90°[d] (E_γ=220–350 MeV)			
TRIUMF (Ref. 8)	3.83	5	6.5%	12%	1.01±0.19
Saclay (Ref. 44)	1.00	8	2.2%	16%	1.24±0.22
Caltech (Ref. 2)	2.08	2	15%	1%	1.60±0.36

[a] Number of degrees of freedom (DF) is one less than the number of data points.
[b] As stated in cited publication.
[c] Ratio to present experiment. Uncertainty includes the uncertainty in fitting the factor A of Eq. (8) (multiplied by $\sqrt{\chi^2/\mathrm{DF}}$ when the latter is >1) and the systematic uncertainties of the experiments.
[d] Multiplied by detailed balance factor.

Craver, Kim, and Tubis[47] performed a calculation using Faddeev three-body wave functions based on the Reid soft core nucleon-nucleon interaction.[48] Above 100 MeV, their cross sections are much lower than experiment, and the angular distribution has an incorrect shape.

Prats[49] found that agreement with experiment near 150 MeV could be obtained by adding a "quasideuteron" diagram to the direct photon-nucleon interaction employed in previous calculations. His calculation has recently been extended[50] to the energy region of the present experiment by the addition of an explicit $\Delta(1232)$ contribution to the photon-deuteron interaction, with a single parameter chosen to give agreement with experimental measurements of deuteron photodisintegration near 250 MeV. The results of this calculation, with and without the $\Delta(1232)$ term, are shown with the data in Fig. 11. The agreement with the results of this experiment is excellent at 60°, but at 90° the calculation appears to overestimate the size of the $\Delta(1232)$ resonant contribution.

In a similar spirit, Fearing has performed a phenomenological calculation using deuteron photodisintegration data as input; his results are plotted in Ref. 8 and are in reasonable agreement with the TRIUMF data.

C. Influence of the $\Delta(1232)$ resonance

Neither the data nor the calculations discussed above exhibit a sharp enhancement at the $\Delta(1232)$ peak energy, in contrast with the cross section for $d(\gamma,p)n$ in this energy region. The calculation of Prats,[49,50] which is plotted in Fig. 11, predicts a larger contribution of the Δ at 90° than at 60°, but the experimental results at 90° show no evidence for this. The relative insignificance of the $\Delta(1232)$ for this reaction is also exhibited by a plot[51] of the square of the invariant matrix element, defined by

$$|M|^2=(8\pi/\hbar c)^2 2(2S_{^3\mathrm{He}}+1)s\frac{k^*}{p^*}\frac{d\sigma}{d\Omega} \tag{9}$$

versus the squared four-momentum transfer t. (s, k^*, and p^* are, respectively, the total center-of-mass energy squared and the photon and proton three-momenta in the center-of-mass system.) Results for our measurements at both angles are shown in Fig. 12. The arrows indicate the t values at which $\sqrt{s}-m_d=1232$ MeV for 60° and 90°. In reactions such as pion photoproduction and deuteron photodisintegration, in which the $\Delta(1232)$ is known to be important, a similar kinematic prescription predicts where the maximum contribution of the $\Delta(1232)$ resonance is to be found,[52] and at such values of t the magnitude of $|M|^2$ is strongly dependent on s. For this experiment, the 60° and 90° data fall on a single curve, indicating that in this energy region the cross section is a function only of t and phase space factors.

D. Conclusions

Our new measurement of $^3He(\gamma,d)p$ is in good agreement with the two most recent measurements of the inverse reaction $d(p,\gamma)^3He$. There is therefore no evidence

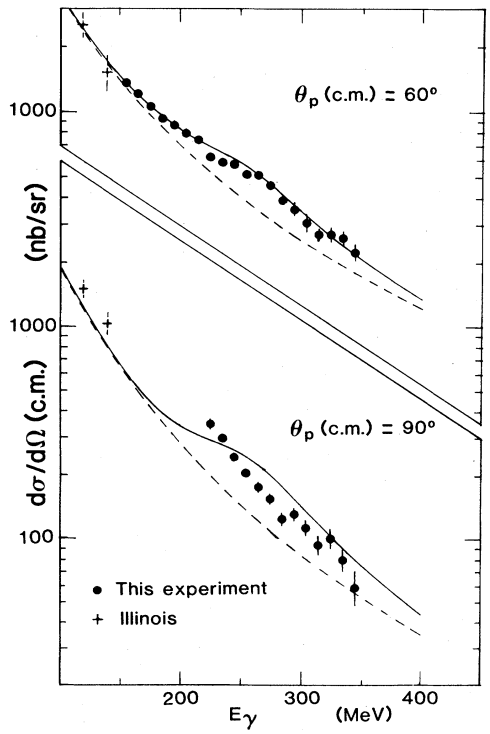

FIG. 11. Cross sections for $\gamma+{}^3He\rightarrow p+d$ measured in this experiment, compared with the theoretical calculation of Prats (Refs. 49 and 50). The solid curves include an explicit $\Delta(1232)$ contribution; the dashed curves show the same calculation with the $\Delta(1232)$ term omitted.

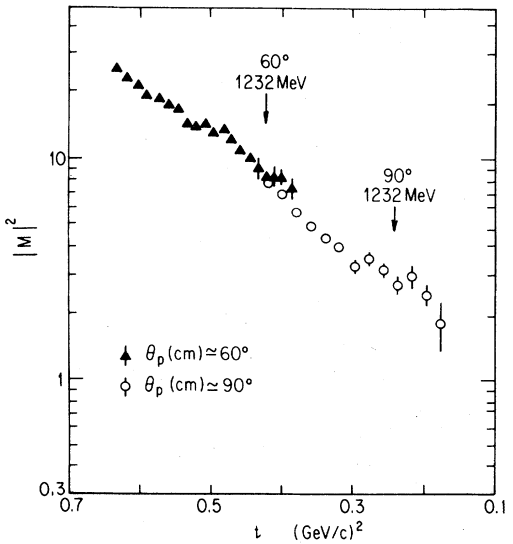

FIG. 12. Invariant matrix element [Eq. (9)] extracted from the cross sections of this experiment, plotted versus invariant momentum transfer squared. The arrows indicate where the maximum contribution of the $\Delta(1232)$ is expected at each angle.

for a violation of detailed balance, although the precision of the test is limited to about 15%, mainly by the systematic uncertainties of the data sets. This is a more precise test of detailed balance than has been obtained in any other electromagnetic process at intermediate energy without bound-nucleon corrections or an arbitrary overall normalization.

Because of uncertainties in the precise role of the $\Delta(1232)$ resonance in this reaction, it is not possible at this time to convert this result to a quantitative test of time-reversal invariance, and we have not attempted to calculate an upper limit on a possible time-reversal-violating phase or other model-dependent parameters. Future theoretical work should make such a calculation possible.

ACKNOWLEDGMENTS

We acknowledge the efforts and support of the linac staff and the (γ,p) group at the MIT Bates Linear Accelerator. We thank N. Kalantar-Nayestanaki, R. S. Turley, B. C. Craft III, and R. Schumacher for their assistance. One of us (D.I.S.) acknowledges the hospitality of the Technische Hochschule Darmstadt and the support of the Deutsche Forschungsgemeinschaft during part of this work. We thank Prof. F. Prats for providing us with the results of his recent calculations. This work was supported in part by U. S. Department of Energy Grants Nos. DE-AT03-81ER40021 and EY-76-C-02-3069, and by National Science Foundation Grant No. PHY-79-23968.

*On leave of absence at the National Science Foundation, Washington, D.C. 20550.

†Present address.

[1]C. A. Heusch, R. V. Kline, K. T. McDonald, and C. Y. Prescott, Phys. Rev. Lett. 37, 405 (1976); K. T. McDonald, Ph.D. thesis, California Institute of Technology, 1972.

[2]C. A. Heusch, R. V. Kline, K. T. McDonald, J. B. Carroll, D. H. Fredrickson, M. Goitein, B. MacDonald, V. Perez-Mendez, and A. W. Stetz, Phys. Rev. Lett. 37, 409 (1976); R. V. Kline, Ph.D. thesis, California Institute of Technology, 1973.

[3]P. Picozza, C. Schaerf, R. Scrimaglio, G. Goggi, A. Piazzoli, and D. Scannicchio, Nucl. Phys. A157, 190 (1970).

[4]N. M. O'Fallon, L. J. Koester, Jr., and J. H. Smith, Phys. Rev. C 5, 1926 (1972).

[5]P. E. Argan, G. Audit, N. De Botton, J.-L. Faure, J.-M. Laget, J. Martin, C. G. Schuhl, and G. Tamas, Nucl. Phys. A237, 447 (1975).

[6]H. J. Gassen, A. Hegerath, W. Loers, B. Mecking, G. Nöldeke, T. Reichelt, and H. Stanek, Z. Phys. A 303, 35 (1981).

[7]B. M. K. Nefkens, Th. S. Bauer, K. Baba, A. Boudard, W. J. Briscoe, G. Bruge, J.-L. Faure, J. Gosset, A. Hegerath, J.-C. Lugol, B. H. Silverman, and Y. Terrien, Phys. Rev. Lett. 45, 168 (1980).

[8]R. Abegg, J. M. Cameron, D. A. Hutcheon, P. Kitching, W. J. McDonald, C. A. Miller, J. W. Pasos, J. Soukup, J. Thekkunthala, H. S. Wilson, A. W. Stetz, and I. J. van Heerden, Phys. Lett. 118B, 55 (1982).

[9]J. Bernstein, G. Feinberg, and T. D. Lee, Phys. Rev. 139, B1650 (1965).

[10]R. L. Anderson, R. Prepost, and B. H. Wiik, Phys. Rev. Lett. 22, 651 (1969).

[11]D. I. Sober, D. G. Cassel, A. J. Sadoff, K. W. Chen, and P. A. Crean, Phys. Rev. Lett. 22, 430 (1969).

[12]P. Dougan, T. Kivikas, K. Lugner, V. Ramsay, and W. Stiefler, Z. Phys. A 276, 55 (1976); P. Dougan, V. Ramsay, and W. Stiefler, *ibid.* 280, 341 (1977).

[13]D. F. Bartlett, C. E. Friedberg, P. E. Goldhagen, and K. Goulianos, Phys. Rev. Lett. 27, 881 (1971).

[14]B. L. Schrock, R. P. Haddock, J. A. Helland, M. J. Longo, S. S. Wilson, K. K. Young, D. Cheng, and V. Perez-Mendez, Phys. Rev. Lett. 26, 1659 (1971).

[15]P. Benz, O. Braun, H. Butenschön, H. Finger, D. Gall, U. Idschok, C. Kiesling, G. Knies, H. Kowalski, K. Müller, B. Nellen, R. Schiffer, P. Schlamp, H. J. Schnackers, V. Schulz, P. Söding, H. Spitzer, J. Stiewe, F. Storim, and J. Weigl, Nucl. Phys. B65, 158 (1973).

[16]G. von Holtey, G. Knop, H. Stein, J. Stümpfig, and H. Wahlen, Nucl. Phys. B70, 379 (1974).

[17]T. Fujii, T. Kondo, F. Takasaki, S. Yamada, S. Homma, K. Huke, S. Kato, H. Okuno, I. Endo, and H. Fujii, Nucl. Phys. B120, 395 (1977).

[18]P. E. Argan, G. Audit, A. Bloch, J.-L. Faure, J.-M. Laget, J. Martin, G. Tamas, and C. Schuhl, Nucl. Phys. A296, 373 (1978).

[19]P. A. Berardo, R. P. Haddock, B. M. K. Nefkens, L. J. Verhey, M. E. Zeller, A. S. L. Parsons, and P. Truoel, Phys. Rev. D 9, 621 (1974).

[20]J. C. Comiso, D. J. Blasberg, R. P. Haddock, B. M. K. Nefkens, P. Truoel, and L. J. Verhey, Phys. Rev. D 12, 719 (1975).

[21]M. T. Tran, L. H. Guex, J. C. Alder, C. Joseph, B. Vaucher, E. Winkelmann, W. Bayer, H. Hilscher, H. Schmitt, C. Zupancic, T. Bressani, E. Chiavassa, J. Favier, D. Schinzel, and P. Truöl, Nucl. Phys. A324, 301 (1979).

[22]W. J. Briscoe, D. H. Fitzgerald, B. M. K. Nefkens, Hall Crannell, D. I. Sober, R. Goloskie, and W. W. Sapp, Jr., Phys. Rev. Lett. 49, 187 (1982).

[23]P. C. Dunn, Nucl. Instrum. Methods 165, 163 (1979).

[24]F. Wolverton, computer program BPAK-I, California Institute of Technology, 1965 (unpublished).

[25]Y. S. Tsai, Rev. Mod. Phys. 46, 815 (1974).

[26]J. L. Matthews and R. O. Owens, Nucl. Instrum. Methods 111, 157 (1973).

[27]H. W. Koch and J. W. Motz, Rev. Mod. Phys. 31, 920 (1959).

[28]P. C. Dunn, S. B. Kowalski, F. N. Rad, C. P. Sargent, W. E. Turchinetz, R. Goloskie, and D. P. Saylor, Phys. Rev. C 27, 71 (1983).

[29]Isotec Inc., 7542 McEwen Rd., Centerville, OH 45459.

[30]W. Bertozzi, M. V. Hynes, C. P. Sargent, W. Turchinetz, and C. Williamson, Nucl. Instrum. Methods 162, 211 (1979).

[31]E. R. Kinney, J. L. Mathews, W. W. Sapp, R. A. Schumacher, and R. O. Owens, Nucl. Instrum. Methods 185, 189 (1981).

[32]W. Bertozzi, M. V. Hynes, C. P. Sargent, C. Creswell, P. C.

Dunn, A. Hirsch, M. Leitch, B. Norum, F. N. Rad, and T. Sasanuma, Nucl. Instrum. Methods 141, 457 (1977).
[33]R. D. Dalitz and D. R. Yennie, Phys. Rev. 105, 1598 (1957).
[34]W. Heitler, *The Quantum Theory of Radiation,* 3rd ed. (Clarendon, Oxford, 1954), p. 378.
[35]R. L. Ford and W. R. Nelson, Stanford University, SLAC Report No. 210, 1978 (unpublished).
[36]J. S. McCarthy, I. Sick, and R. R. Whitney, Phys. Rev. C 15, 1396 (1977).
[37]Z. M. Szalata, J. M. Finn, J. Flanz, F. J. Kline, G. A. Peterson, J. W. Lightbody, Jr., X. K. Maruyama, and S. Penner, Phys. Rev. C 15, 1200 (1977).
[38]G. R. Bishop, M. Bernheim, and P. Kossanyi-Demay, Nucl. Phys. 54, 353 (1964).
[39]E. B. Dally, M. G. Croiseaux, and B. Schweitz, Phys. Rev. C 2, 2057 (1970).
[40]J. Arends, H. J. Gassen, A. Hegerath, B. Mecking, G. Nöldeke, P. Prenzel, T. Reichelt, A. Voswinkel, and W. W. Sapp, Nucl. Phys. A (to be published).
[41]J. Arends, J. Eyink, A. Hegerath, H. Hartmann, B. Mecking, G. Nöldeke, and H. Rost, Nucl. Phys. A322, 253 (1979).
[42]R. E. Segel, T. Chen, L. L. Rutledge, Jr., J. V. Maher, J. Wiggins, P. P. Singh, and P. T. Debevec, Phys. Rev. C 26, 2424 (1982).
[43]J. Källne, J. E. Bolger, M. J. Devereaux, and S. L. Verbeck, Phys. Rev. C 24, 1102 (1981).
[44]B. H. Silverman, Ph.D. thesis, University of California, Los Angeles, 1983 (unpublished); B. H. Silverman, A. Boudard, W. J. Briscoe, G. Bruge, P. Couvert, L. Farvacque, D. H. Fitzgerald, C. Glashausser, J.-C. Lugol, and B. M. K. Nefkens (unpublished).
[45]J. Finjord, Nucl. Phys. A274, 495 (1976).
[46]G. F. Chew, M. L. Goldberger, F. E. Low, and Y. Nambu, Phys. Rev. 106, 1345 (1957).
[47]B. A. Craver, Y. E. Kim, and A. Tubis, Nucl. Phys. A276, 237 (1977).
[48]R. V. Reid, Jr., Ann. Phys. (N.Y.) 50, 411 (1968).
[49]F. Prats, Phys. Lett. 88B, 23 (1979).
[50]F. Prats (private communication).
[51]B. M. K. Nefkens, *Proceedings of Symposium on Δ-Nucleus Dynamics, Argonne, 1983* (unpublished).
[52]B. M. K. Nefkens, *Abstracts of the Proceedings of the Ninth International Conference on High Energy Physics and Nuclear Structure, Versailles, 1981,* edited by P. Catillon, P. Radvanyi, and M. Porneuf (North-Holland, Amsterdam, 1982), p. 199, and summarized by P. L. Walden, Nucl. Phys. A374, 277c (1982).